Galayda A. P., Volkova N. E., Dyagileva A. I.,
Gavrilova L. Ya., Cherepanov V. A., Battle P. D.
Chimica Techno Acta. 2018. Vol. 5, No. 4. P. 159–165.
ISSN 2409–5613

DOI: 10.15826/chimtech.2018.5.4.01

A. P. Galayda[a*], N. E. Volkova[a], A. I. Dyagileva[a], L. Ya. Gavrilova[a], V. A. Cherepanov[a], P. D. Battle[b]

[a] *Institute of Natural Sciences and Mathematics, Ural Federal University, 19 Mira St., Ekaterinburg, 620002, Russian Federation*
[b] *Inorganic Chemistry Laboratory, University of Oxford, South Parks Road, Oxford OX1 3QR, UK*
**E-mail: anastasia.galaida@urfu.ru*

Crystal structure and properties of novel oxide $Sm_{0.9}Ca_{1.1}Fe_{0.7}Co_{0.3}O_{4-\delta}$

$Sm_{0.9}Ca_{1.1}Fe_{0.7}Co_{0.3}O_{4-\delta}$ oxide with the K_2NiF_4-type structure was prepared using a glycerin-nitrate technique. The XRD pattern of $Sm_{0.9}Ca_{1.1}Fe_{0.7}Co_{0.3}O_{4-\delta}$ was refined by the Rietveld method within an orthorhombic structure (space group *Bmab*). The electrical conductivity, Seebeck coefficient, and thermal expansion of $Sm_{0.9}Ca_{1.1}Fe_{0.7}Co_{0.3}O_{4-\delta}$ were measured depending on temperature in air. The change of oxygen nonstoichiometry determined by TGA in air does not exceed 0.01. The oxygen content in $Sm_{0.9}Ca_{1.1}Fe_{0.7}Co_{0.3}O_{4-\delta}$ determined by the reduction in a hydrogen flux is equal to 3.96 ± 0.01. The positive value of Seebeck coefficient indicates that the predominant charge carriers in the oxide studied are electron holes.

Keywords: complex oxide; Ruddlesden-Popper phase; crystal structure; oxygen nonstoichiometry, electroconductivity; thermal expansion.

Received: 13.11.2018. Accepted: 05.12.2018. Published: 31.12.2018.

© Galayda A. P., Volkova N. E., Dyagileva A. I., Gavrilova L. Ya., Cherepanov V. A., Battle P. D., 2018

Introduction

Complex oxides with the K_2NiF_4-type structure based on rare earth, alkaline earth and 3d-transition metals are known as materials with high mixed electronic-ionic conductivity and oxygen mobility, and also thermodynamic stability at high temperature under an oxidizing atmosphere [1–4]. For this reason, K_2NiF_4-type oxides have attracted much attention as promising SOFC cathodes [1–3], oxygen-separation membranes [5] and catalysts [6]. The crystal structure of a K_2NiF_4-type oxide is built up by alternating the perovskite layer (ABO_3) and rock salt layer (AO) [7]. Depending on the nature of the metals in the A and B sublattices, the crystal structure of oxides with overall composition A_2BO_4 can be described using a tetragonal (sp. gr. *I4/mmm*) or orthorhombic (sp. gr. *Bmab*) unit cell [3–13]. Compared with Sr-substituted phases, very little is known about Ca-doped analogues with the K_2NiF_4-type structure. It has been reported previously that metastable lanthanum calcium ferrite $CaLaFeO_{4-\delta}$ decomposes at 1100 °C to lanthanum ferrite $LaFeO_{3-\delta}$ and calcium oxide CaO [14]. One can expect that variation of the Ln/Ca ratio and partial substitution of more electronegative Co for Fe ions

in the B-site position will stabilize the K_2NiF_4-type structure. The present study has focused on the structure and properties of the novel $Sm_{0.9}Ca_{1.1}Fe_{0.7}Co_{0.3}O_{4-\delta}$ oxide with the K_2NiF_4-type structure.

Experimental

The complex oxide was prepared using a glycerin nitrate technique. Samarium oxide Sm_2O_3 (99.99% purity), calcium carbonate $CaCO_3$ ("pure for analysis" grade), metallic cobalt Co, iron oxalate $FeC_2O_4{\cdot}2H_2O$ ("pure for analysis" grade), nitric acid ("special purity" grade) and glycerin were used as the starting materials. Metallic cobalt was obtained by reducing cobalt oxide Co_3O_4 ("special purity" grade) in the hydrogen flow at 400–600 °C for 6 h. The appropriate stoichiometric amounts of starting materials were dissolved in nitric acid, and then glycerin was added to the solution. The resulting gel was dried in a porcelain cup, decomposed to the dark powder, then placed in an alumina crucible and calcined in air at 700–1000 °C for 8–10 h. The final annealing was performed at 1100 °C in air for 120 h with intermediate grindings, followed by slow cooling to room temperature at a rate of ~100 °C/h. The phase composition of the annealed samples was determined by X-ray diffraction using a Shimadzu XRD-7000 (CuKα-radiation, angle range 2Θ = 20–90°, step 0.03°, 5 s/step) in air. The structural parameters were refined by the Rietveld profile method using the Fullprof-2008 package. Thermogravimetric analysis (TGA) was carried out using an STA 409 PC instrument (Netzsch) over the temperature range 25–1100 °C in air in dynamic (heating/cooling rate 2 K/min) mode. The absolute values of oxygen content were determined by a reduction of the samples in a hydrogen flux inside the TGA cell at 1200 °C [15]. Thermal expansion measurements were carried out within the temperature range of 25–1100 °C in air using a dilatometer DIL 402C (Netzsch) at a heating/cooling rate of 5K/min. The total conductivity and Seebeck coefficients of ceramic samples were measured in air by a 4-probe method with platinum electrodes. A bar-shaped sample (3×4×25 mm) for thermal expansion coefficient (TEC) and conductivity measurements was obtained by pressing powder that was mixed with 2–3 drops of ethanol using a manually-operated press. Afterwards, the samples prepared accordingly were slow heated and then sintered at 1200 °C for 14 h in air followed by slow cooling (the rate of heating and cooling was 50 K/h). The relative density of the sample was evaluated by a comparison of measured values to those calculated from the XRD-data. The relative density was found to be 90%.

Results and discussion

In contrast with previously reported $SmCaCoO_{4-\delta}$ [10] and $LnSrFeO_{4-\delta}$ (Ln=La [16], Nd [17, 18], Gd [19], Sm [13]), we have failed to synthesize samarium-calcium ferrite with an equimolar Sm/Ca-ratio at 1100 °C in air. It is known that the homogeneity range limits for such solid solutions depend significantly on temperature, ionic radius of dopants and oxygen partial pressure. The decrease of temperature from 1500 °C to 1100 °C leads to decomposition of $CaLaFeO_{4-\delta}$ to $LaFeO_{3-\delta}$ and CaO [14].

The complex oxide $Sm_{0.9}Ca_{1.1}Fe_{0.7}Co_{0.3}O_{4-\delta}$ was prepared

by a standard glycerin-nitrate technique with annealing temperature 1100 °C in air. Diffraction data for $Sm_{0.9}Ca_{1.1}Fe_{0.7}Co_{0.3}O_{4-\delta}$ analyzed by the Rietveld method are shown in Fig. 1. XRD pattern of $Sm_{0.9}Ca_{1.1}Fe_{0.7}Co_{0.3}O_{4-\delta}$ was indexed in the orthorhombic structure (sp. gr. *Bmab*).

The value of the oxygen content in $Sm_{0.9}Ca_{1.1}Fe_{0.7}Co_{0.3}O_{4-\delta}$ at room temperature determined by the TGA reduction was found to be 3.96 ± 0.01, and is consistent with that for $SmCaCoO_{4-\delta}$ [10]. The TGA measurements within the temperature range of 25–1100 °C in air revealed a small change in oxygen content, 4-δ, that is less than 0.01 (Fig. 2).

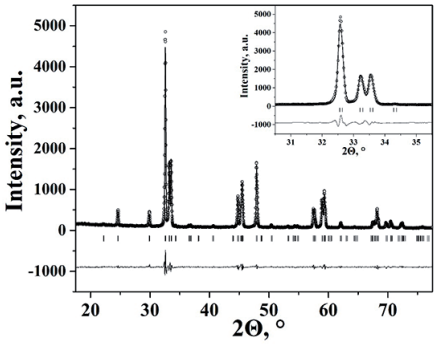

Fig. 1. Rietveld refined XRD pattern of $Sm_{0.9}Ca_{1.1}Fe_{0.7}Co_{0.3}O_{4-\delta}$. Circles are the experimental XRD data, upper continuous line is the calculated profile, lower continuous line is the difference plot, vertical lines are indicating the Bragg positions

The temperature dependence of the thermal expansion in air for $Sm_{0.9}Ca_{1.1}Fe_{0.7}Co_{0.3}O_{4-\delta}$ is given in Fig. 3 in comparison with $SmCaCoO_{4-\delta}$ [10].

As can be seen, the shape of the measured dependence is non-linear. Since this phenomenon cannot be explained by a noticeable oxygen exchange, we suggest that the non-linearity of the dilatometric plot is mainly associated with redistribution of electron density between Co and Fe and/or changes in Co spin states with the temperature. Similar behavior was observed in $SmFe_{1-x}Co_xO_{3-\delta}$ (x = 0.2, 0.5, 0.8) [10]. However, additional research is needed to clarify this behavior. The dependence of $\Delta L/L=f(T)$ has been described by two linear equations in the temperature ranges of 25–400 °C and 730–1000 °C. Low- and high-temperature TEC values for $Sm_{0.9}Ca_{1.1}Fe_{0.7}Co_{0.3}O_{4-\delta}$ in comparison with those of $SmCaCoO_{4-\delta}$ and most common SOFC electrolytes are listed in Table 1. The decrease in the TEC value with the increase of iron content can be explained by the higher bond energy

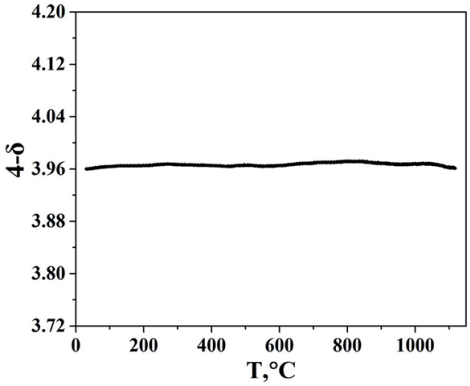

Fig. 2. Oxygen content, 4–δ, in $Sm_{0.9}Ca_{1.1}Fe_{0.7}Co_{0.3}O_{4-\delta}$ as a function of temperature in air

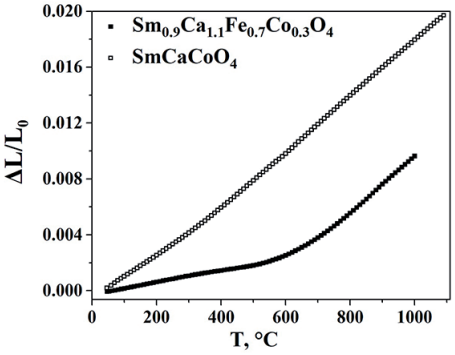

Fig. 3. Thermal expansion of the $Sm_{0.9}Ca_{1.1}Fe_{0.7}Co_{0.3}O_{4-\delta}$ and $SmCaCoO_{4-\delta}$ [10] ceramics in air

Table 1

The average thermal expansion coefficients for $Sm_{0.9}Ca_{1.1}Fe_{0.7}Co_{0.3}O_{4-\delta}$, $SmCaCoO_{4-\delta}$ [10] and SOFC electrolytes $Zr_{0.85}Y_{0.15}O_{2-\delta}$ [22] and $Ce_{0.8}Sm_{0.2}O_{2-\delta}$ [23] in air

Composition	Temperature range, °C	TEC×10^6, K^{-1}
$Sm_{0.9}Ca_{1.1}Fe_{0.7}Co_{0.3}O_{4-\delta}$	25–400	4.4
	730–1000	20.2
$SmCaCoO_{4-\delta}$ [10]	25–580	17.7
	580–1100	20.2
$Zr_{0.85}Y_{0.15}O_{2-\delta}$ [22]	30–1000	10.9
$Ce_{0.8}Sm_{0.2}O_{2-\delta}$ [23]	30–1000	12.5

for Fe–O (409 kJ/mol) compared to Co–O (368 kJ/mol) [20].

The total conductivity of $Sm_{0.9}Ca_{1.1}Fe_{0.7}Co_{0.3}O_{4-\delta}$ versus temperature is shown in Fig. 4.

The conductivity of $Sm_{0.9}Ca_{1.1}Fe_{0.7}Co_{0.3}O_{4-\delta}$ monotonously increases with temperature up to 23 S/cm at 1100 °C. In contrast, the Seebeck coefficient decreases with temperature. The positive value of the Seebeck coefficient (see Fig. 5) indicates that electron holes are the predominant charge carriers in the oxide studied. The conductivity activation energies calculated from two linear segments of Arrhenius plot (see insert in Fig. 4) are equal to 0.193 eV and 0.283 eV in the temperature ranges 50–250 °C and 300–1100 °C, respectively. Both values are typical for a hopping conduction mechanism.

A comparison of the temperature dependences of the total conductivity of $Sm_{0.9}Ca_{1.1}Fe_{0.7}Co_{0.3}O_{4-\delta}$ and $SmCaCoO_{4-\delta}$ [10] (see Fig. 4) visually shows that they coincide in practical term up to 600 °C and the conductivityhas thermally activated character for both oxides. A strong increase in the conductivity of $SmCaCoO_{4-\delta}$ above 600 °C can be explained by the pronounced charge disproportionation process at higher temperatures:

$$2Co_{Co}^{\times} \leftrightarrow Co_{Co}^{\circ} + Co_{Co}' \qquad (1)$$

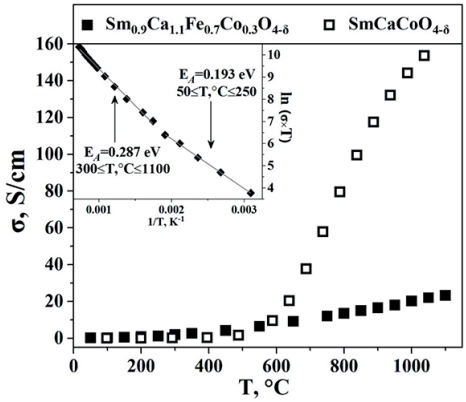

Fig. 4. Total conductivity of $Sm_{0.9}Ca_{1.1}Fe_{0.7}Co_{0.3}O_{4-\delta}$ and $SmCaCoO_{4-\delta}$ [10] versus temperature in air. The insert shows the Arrhenius plot for $Sm_{0.9}Ca_{1.1}Fe_{0.7}Co_{0.3}O_{4-\delta}$

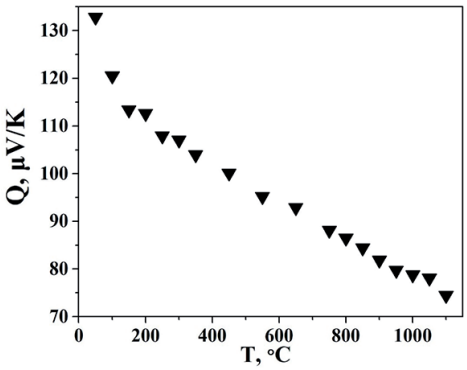

Fig. 5. Seebeck coefficient for $Sm_{0.9}Ca_{1.1}Fe_{0.7}Co_{0.3}O_{4-\delta}$ vs. temperature in air

In contrast, simultaneous presence of Co and Fe at the B-sites suppress disproportionation of iron and cobalt by the following process:

$$Fe^{\times}_{Fe} + Co^{\times}_{Fe} \leftrightarrow Fe^{\circ}_{Fe} + Co'_{Fe}, \quad (2)$$

where iron seems to be a hole trap [21].

Conclusions

Single-phase $Sm_{0.9}Ca_{1.1}Fe_{0.7}Co_{0.3}O_{4-\delta}$ was successfully synthesized by a glycerin nitrate technique. The structural parameters of the oxide prepared were refined by the Rietveld method. The oxygen content, 4–δ, at room temperature was found to be 3.96 ± 0.01 and its decrease with temperature does not exceeded 0.01. The lower value of the total conductivity of $Sm_{0.9}Ca_{1.1}Fe_{0.7}Co_{0.3}O_{4-\delta}$ compared to that of $SmCaCoO_{4-\delta}$ was explained in terms of an electronic exchange process. The Seebeck coefficient of $Sm_{0.9}Ca_{1.1}Fe_{0.7}Co_{0.3}O_{4-\delta}$ was shown to be positive over the entire temperature range investigated, indicating predominantly p-type conductivity.

Acknowledgements

This work was supported in parts by Act 211 Government of the Russian Federation, agreement 02.A03.21.0006.

References

1. Istomin SYa, Antipov EV. Cathode materials based on perovskite-like transition metal oxides for intermediate temperature solid oxide fuel cells. *Russ Chem Rev.* 2013;82(7):686–700. DOI: 10.1070/RC2013v082n07ABEH004390.
2. Dailly J, Fourcade S, Largeteau A, Mauvy F, Grenier JC, Marrony M. Perovskite and A_2MO_4-type oxides as new cathode materials for protonic solid oxide fuel cells. *Electrochim Acta.* 2010;55(20):5847–53. DOI: 10.1016/j.electacta.2010.05.034.
3. Zhao F, Wang X, Wang Z, Peng R, Xia C. K_2NiF_4 type $La_{2-x}Sr_xCo_{0.8}Ni_{0.2}O_{4+\delta}$ as the cathodes for solid oxide fuel cells. *Solid State Ionics.* 2008;179:1450–3. DOI: 10.1016/j.ssi.2008.06.019.
4. Daroukh MAl, Vashook VV, Ullmann H, Tietz F, Arual Raj I. Oxides of the AMO_3 and A_2MO_4-type: structural stability, electrical conductivity and thermal expansion. *Solid State Ionics.* 2003;158:141–50. DOI: 10.1016/S0167-2738(02)00773–7.
5. Vashook VV, Yushkevich II, Kokhanovsky LV, Makhnach LV, Tolochko SP, Kononyuk IF, Ullmann H, Altenburg H. Composition and conductivity of some nickelates. *Solid State Ionics.* 1999;119:23–30. DOI: 10.1016/S0167-2738(98)00478–0.
6. Ling Z, Xuezhong W, Cunzhen L. Catalytic combustion of diesel soot over K_2NiF_4-type oxides $La_{2-x}K_xCuO_4$. *J Rare Earths.* 2008.;26(2):254–7. DOI: 10.1016/S1002-0721(08)60076–9.
7. Skinner SJ. Characterisation of $La_2NiO_{4+\delta}$ using in-situ high temperature neutron powder diffraction. *Solid State Sci.* 2003;5:419–26. DOI: 10.1016/S1293-2558(03)00050–5
8. Taguchi H, Nakade K, Hirota K. Synthesis and characterization of K_2NiF_4-type $CaLnCoO_4$ (Ln = Sm and Gd). *Mater Res Bull.* 2007;42:649–56. DOI: 10.1016/j.materresbull.2006.08.004.

9. Taguchi H, Kido H, Tabata T. Relationship between crystal structure and electrical property of K_2NiF_4-type $(Ca_{1-x}Nd_{1+x})CoO_{4-d}$. *Physica B.* 2004;344:271–7. DOI: 10.1016/j.physb.2003.09.270.
10. Galayda AP, Volkova NE, Gavrilova LYa, Balymov KG, Cherepanov VA. Phase equilibria, structure and properties of intermediate phases in the Sm_2O_3-Fe_2O_3-CoO and Sm_2O_3-CaO-CoO systems. *J Alloys Compd.* 2017;718:288–97. DOI: 10.1016/j.jallcom.2017.05.044.
11. Romero de Paz J, Fernández-Díaz MT, Hernández Velasco J, Sáez Puche R, Martinez JL. Crystal and Magnetic Structure of $PrCaCrO_4$. *J Solid State Chem.* 1999;142(1):29–32. DOI: 10.1006/jssc.1998.7973.
12. Thorogood GJ, Orain P-Y, Ouvry M, Piriou B, Tedesco T, Wallwork KS, Herrmann J, James M. Structure, crystal chemistry and magnetism of rare earth calcium-doped cobaltates: $Ln_{2-x}Ca_xCoO_{4+\delta}$ (Ln=Pr, Nd, Sm, Eu, Gd). *Solid State Sci.* 2011;13:2113–23. DOI: 10.1016/j.solidstatesciences.2011.08.008.
13. Volkova NE, Maklakova AV, Gavrilova LYa, Cherepanov VA. Phase equilibria, crystal structure, and properties of intermediate oxides in the Sm_2O_3–SrO–CoO system. *Eur J Inorg Chem.* 2017:3285–92. DOI: 10.1002/ejic.201700321.
14. Nguyen-Trut-Dinh MM, Vlasse M, Perrin M, Le Flem G. Un oxide magnetique bidimensionnel: $CaLaFeO_4$. *J Solid State Chem.* 1980;32:1–8. DOI: 10.1016/0022–4596(80)90262–5.
15. Volkova NE, Gavrilova LYa, Cherepanov VA, Aksenova TV, Kolotygin VA, Kharton VV. Synthesis, crystal structure and properties of $SmBaCo_{2-x}Fe_xO_{5+\delta}$. *J Solid State Chem.* 2013:204;219–23. DOI: 10.1016/j.jssc.2013.06.001.
16. Jennings AJ, Skinner SJ, Helgason Ö. Structural properties of $La_xSr_{2-x}FeO_{4\pm d}$ at high temperature and under reducing conditions. *J Solid State Chem.* 2003;175:207–17. DOI: 10.1016/S0022-4596(03)00248–2.
17. Ki-Woog S, Ki-Tae L. Characterization of $NdSrCo_{1-x}Fe_xO_{4+d}$ ($0 \le x \le 1.0$) intergrowth oxide cathode materials for intermediate temperature solid oxide fuel cells. *Ceram Int.* 2011;37:573–7. DOI: 10.1016/j.ceramint.2010.10.004.
18. Aksenova TV, Vakhromeeva AE, Elkalashy ShI, Urusova AS, Cherepanov VA. Phase equilibria, crystal structure, oxygen nonstoichiometry and thermal expansion of complex oxides in the Nd_2O_3–SrO–Fe_2O_3 system. *J Solid State Chem.* 2017;251:70–8. DOI: 10.1016/j.jssc.2017.04.015.
19. Singh S, Singh D. Effect of increasing Sr content on structural and physical properties of K_2NiF_4-type phase $GdSrFeO_4$. *Ceram Int.* 2017;43:3369–76. DOI: 10.1016/j.ceramint.2016.11.182.
20. Cottrell TL. The Strengths of Chemical Bonds. 2nd ed. London: Butterworth; 1958. 317 p.
21. Tai L-W, Nasrallah MM, Anderson HU, Sparlin DM, Sehlin SR. Structure and electrical properties of $La_{1-x}Sr_xCo_{1-y}Fe_yO_3$. Part 1. The system $La_{0.8}Sr_{0.2}Co_{1-y}Fe_yO_3$. *Solid State Ionics.* 1995;76:259–71. DOI: 10.1016/0167–2738(94)00244-m.
22. Tsipis EV, Kharton VV. Electrode materials and mechanisms in solid oxide fuel cells: brief review. *J Solid State Electrochem.* 2008;12(11):1367–91. DOI: 10.1007/s10008-008-0611-6.

23. Pikalova EYu, Murashkina AA, Maragou VI, Demin AK, Strekalovsky VN, Tsiakaras PE. CeO_2 based materials doped with lanthanides for applications in intermediate temperature electrochemical devices. *Int J Hydrogen Energy.* 2011;36:6175–83. DOI: 10.1016/j.ijhydene.2011.01.132.